Prediction of Freshwater Production in Seawater Greenhouses Using Hybrid Models of Artificial Neural Network

Abstract

Freshwater production plays a critical role in the era of water shortage and persistent droughts. One of the methods of freshwater production is the use of seawater greenhouse (SSGH), which desalinates saline water using solar energy and is an effective method for meeting agricultural irrigation demands. This study predicted the freshwater production in an SSGH in Oman using the artificial neural network (ANN) model. Freshwater production was predicted using greenhouse length and width, roof transparency coefficient, and height of front evaporator. The ANN model was trained using ant-lion optimization (ALO) algorithm, particle swarm optimization (PSO) algorithm, and bat algorithm (BA). Examination of input parameters revealed that the width of the greenhouse was the most critical parameter among the input parameters. Comparison of models showed that the ANN-ALO model had the highest accuracy. Root mean square error (RMSE), mean absolute error (MAE), Percent bias (PBIAS), and Nash Sutcliffe efficiency (NSE) indices were evaluated for each model. Results showed that the RMSE value of the ANN-ALO model was 0.545 m^3 / day. The lowest RMSE was attained by the ANN-ALO in the training and testing phases among the other models. The RMSE value of the ANN-ALO model was 17%, 36%, and 40% lower than ANN-BA, ANN-PSO, and ANN models, respectively. Outputs of the training phase revealed that the ANN-ALO model had the lowest MAE value. Also, the study performed an uncertainty analysis, considering the uncertainty of predictive models for two scenarios: (1) the uncertainty of inputs and (2) uncertainty of model parameters. The uncertainty of ANN-ALO was lower than those of other models in both

scenarios. The investigation of the effect of varying parameters on freshwater production showed that the increase in the width of the greenhouse with an evaporator height of 2 m and a transparency coefficient of 0.4 at a fixed length of 50 m led to an increase in freshwater production. Furthermore, the greenhouse freshwater production with an evaporator height of 2 m and a transparency coefficient 0.4 increased with an increase in width along the length of 100 m. The outputs of models showed that the ANN-ALO model was capable of predicting the amount of fresh water.

Keywords: ANN, optimization algorithm, seawater greenhouse, water production

Introduction

Nowadays, the world is facing a water supply crisis because of population growth, frequent droughts, and lack of enough water resources. Optimal management and utilization of water resources can augment water supplies.

Food security depends on agricultural production, which needs enough water for irrigation. Desalination is one of the useful methods for producing freshwater (Zarei et al., 2018). Although membrane and reverse osmosis technologies are widely used to desalinate brackish water, they entail very high energy cost. Another convenient and low-cost method of producing freshwater for agriculture and irrigation is the use of SSGH, which involves low installation and operating costs (Zarei and Behyad, 2019). SSGH produces freshwater using renewable energies. SSGH is a kind of desalination plant that uses solar energy with high energy savings and seawater (SW) to humidify the air inside the greenhouse and produce freshwater (Essa et al., 2020). Since it uses fewer mechanical parts and has lower maintenance costs, it is more cost-effective than other desalination plants (Essa et al., 2020). Also, it can be used for producing water in hot and dry areas. An SSGH has two cooling evaporators (EV), a condenser, a fan, seawater (SW) pipes,

47 distilled water, and crops between EVs. In the first step, the incoming warm air enters the
48 greenhouse by fans. Then, the incoming warm air moves through the first evaporator (Zarei and
49 Behyad, 2019). Because of the heat exchange with SW in the first evaporator, the inlet hot air
50 temperature decreases and the relative humidity increases. Cool and humid air (HA) enters the
51 greenhouse in the next stage. The greenhouse space is heated by sunlight. In the greenhouse, the
52 solar radiation warms the air inside the greenhouse. The seawater leaves the first evaporator to
53 fall on the second evaporator (Figure 1).

54 Solar absorbing tubes placed on the roof of the greenhouse are used as an energy source
55 for desalination (Zarei et al., 2018). As the air inside the greenhouse has low humidity, it is
56 impossible to separate water. Thus, the air passes through the second evaporator to reduce its
57 temperature and increase its humidity. Then, the air enters a condenser that produces freshwater
58 Part of the water is used to meet the water needs of greenhouse produce, and the other part is
59 used for drinking.

60 Goosen et al. (2003) experimentally evaluated the effect of various SSGH parameters on
61 freshwater production and showed that greenhouse dimensions significantly affected freshwater
62 production and energy consumption. Tahri et al. (2009) proposed a mathematical model for
63 estimation of mass condensation rate of the SSGH in Oman. This model used the heat balance of
64 all heat sources to estimate mass condensation rate. It was concluded that solar radiation was the
65 most important parameter that affected the performance of the SSGH. Mahmoudi et al. (2010)
66 investigated the effect of the passive condenser on SSGH to produce freshwater. They found that
67 using a passive condenser increased the production of freshwater compared to using a pump-
68 driven system. Al-Khalidi et al. (2010) conducted a study to test the performance of a plate-
69 channel condenser (PCC) and a vibrating-surface condenser (VSS) in the SSGH. They found

70 that the freshwater production of the PCC was more that of the VSS. Yetilmezsoy et al. (2014)
71 used an experimental model to estimate the mass condensate flux in SSGH. Without
72 computational complexities, they calculated the mass flux values for various inputs like wet air
73 inlet temperature, moist air, relative humidity, dry inlet air, inlet seawater temperature, and wet
74 air mass flow. Tahri et al. (2016) proposed a multiple linear regression (MLR) model to estimate
75 the dehumidification rate of the condenser. It was observed that the MLR was more accurate
76 compared to the other models. Al-Ismaili et al. (2019) developed the ANN and MLR models for
77 estimation of freshwater production. It was observed that the ANN outperformed the other
78 models.

79 The key parameter in an SSGH is the freshwater production, which is a function of different
80 parameters like climatic parameters and geometric characteristics of the greenhouse. Despite the
81 advantages of the hydrodynamic and mathematical models in predicting freshwater production,
82 they had disadvantages. Implementing complex boundary conditions and preparing a large
83 number of data are the disadvantages of these models (Zarei and Behyad, 2019). These models
84 mainly suffer from high computational time and computational complexity. Thus, it is necessary
85 to develop new models as alternatives to thermodynamic and mathematical models. Recently,
86 soft computing models have been successfully used in various fields. Soft computing models can
87 accurately predict target variables using training data with various training algorithms. These
88 models can detect nonlinear and complex relationships between target variables and inputs for a
89 variable number of inputs.

90 The application of soft computing models is not limited to a special filed. For example,
91 soft computing models are widely used for the estimation of solar radiation in renewable energy
92 applications. Notton et al. (2018) used the ANN model for estimation of Global horizontal

93 irradiation. For the developed ANN model, the normalized RMSE varied from 22.57% to
94 34.85%. Jahani and Mohammadi et al. (2018) coupled the ANN model with the genetic
95 algorithm to estimate daily global solar radiation in Iran. The results indicated that the coupled
96 ANN model performed better than the ANN model. Ghimre et al. (2019) compared the accuracy
97 of the ANN, support vector machine (SVM), genetic programming (GP), and Gaussian process
98 machine learning (GPML) to estimate daily solar radiation. They found that the accuracy of the
99 ANN model was better than those of the other models. Also, soft computing models are widely
100 used for modelling hydrological variables. Sharghi et al. (2018) used the wavelet emotional
101 ANN for one-time-ahead rainfall-runoff modeling. It was concluded that the WANN performed
102 better than the emotional ANN. Kumar et al. (2019) conducted a study for rainfall-runoff
103 modelling that compared two types of the ANN model. The results indicated that the emotional
104 ANN outperformed the ANN model. Qasem et al. (2019) compared the accuracy of the ANN,
105 SVM, wavelet SVM, and wavelet ANN to estimate evaporation. The results of the study
106 indicated that the ANN and wavelet ANN outperformed the SVM and wavelet SVM model.
107 Singh et al. (2019) used ANN and multiple linear regression to predict evaporation. Based on the
108 comparison, the ANN model was superior to the multiple linear regression. Samantaray et al.
109 (2020) compared the performance of the ANN, adaptive neuro-fuzzy interface system (ANFIS),
110 and SVM to estimate rainfall. The results indicated that the accuracy of the SVM model was
111 better than those of the other models. Malik et al. (2020) developed a study based on multi-gene
112 genetic programming (MGGP), SVM, and some types of ANN to predict monthly evaporation.
113 The results indicated that the ANN and MGGP gave accurate results. Several studies used soft
114 computing models for prediction of different variables in SSGHs. Zarei et al. (2018) applied the
115 support vector machine (SVM) model to predict the freshwater produced in an SSGH in Oman.

116 They indicated that SVR had a high capability for predicting freshwater production using data
117 training and various kernel functions.

118 Al-Ismaili et al. (2018) used a multiple linear regression model to estimate the rate of
119 condenser dehumidification in an SSGH in Oman. Using the mass flow rate, inlet humid air
120 temperature (IMAT), inlet humidity ratio (HR), and solar radiation as input data, they showed
121 that the proposed model was accurate in estimating the dehumidification rate. Zarei and Behyad
122 (2019) used ANN to predict freshwater production in an SSGH in Oman. ANN was found
123 accurate in simulating the water produced in the greenhouse. Using solar radiation, IMAT, HR,
124 and mass flow rate as inputs, Al-Ismaili et al. (2019) used ANN and multiple-regression to
125 predict freshwater production in SSGH, and showed that ANN more accurately estimated the
126 freshwater production than did multiple-regression. Essa et al. (2020) used the random vector
127 functional link model (RVFL) and optimization algorithms to predict the freshwater production
128 and energy consumption in SSGH and showed that combination of RVFL model and
129 optimization algorithms better predicted the water produced as well as the energy consumed.
130 Successful experience of using soft computing models shows that they are reliable for predicting
131 different variables.

132 ANN models are one of the most successful models of soft computing models. ANN can
133 estimate target variables using computational multilayers and neurons. They can predict various
134 variables with high accuracy. Although the ANN model can predict different variables, it has
135 some weaknesses. One of the weaknesses is finding model parameters (Shargi et al., 2019).
136 Model parameters like weight connections and bias must be calculated accurately. Although the
137 model uses various training algorithms to find parameters, these algorithms may fall in local
138 optimization trap or have a low convergence rate (Shargi et al., 2019). One way to modify the

ANN model is to connect the model to optimization algorithms. Given robust operators, high convergence speed and high accuracy, optimization algorithms can find the exact value of ANN model parameters. ALO is one of the new optimization algorithms. ALO is widely used in various fields of optimization, as shown in Table 1. Given its high convergence speed, advanced operators to get out of local optima, high accuracy in finding the global optimal solution response, and high flexibility to connect to soft computing models (Mirjalili, 2015). Thus, the study used the ANN-ALO model to estimate the production of freshwater in an SSGH in Oman. Moreover, two other optimization algorithms, called bat and PSO algorithms, were used to train the ANN model in assessing the potential of the ANN-ALO model. While a number of the previous researches uses the mathematical and thermodynamic models for predicting freshwater production, the present study develops soft computing models without using climatic parameters to predict freshwater production.

Investigating the effect of different sources of uncertainty on the accuracy of the models is another innovation of the current paper. Also, new hybrid models of the present study can be used to predict other hydrological variables in the next researches. Thus, the second part of the study describes the ANN model and optimization algorithms. The third part describes a case study and details of SSGH. Part four describes the output. Finally, part five states the conclusion. In addition to using ANN hybrid models to predict freshwater production, the study examined the effect of different parameters on the production of freshwater.

2. Materials and methods

2.1. ANN Model

ANN is inspired by the neural network of the human brain. Each ANN model has computational units called neurons which are seen in different ANN layers (Mirarabi et al., 2019). Each ANN

model has three layers. The first layer is the input data receiving layer, the second layer is known as the hidden layer, and the last layer is the output layer (Jahani and Mohammadi, 2019). The neurons of the first layer are equal to the number of input data (Yadav et al., 2020). The layers connected to the previous and next layers through weighted connections. The number of output layer neurons is equal to the number of ANN model outputs.

The number of hidden layer neurons can be calculated by trial and error. The output of each layer is the input of the next layer. Figure 2 shows the structure of the ANN model. The input values per neuron are multiplied by a weight and enter into the activation function after being summed with a constant value as bias.

One of the most effective training methods of ANN is the backpropagation algorithm (BPA). In BPA, the first level is the feedforward phase (Moghaddam et al., 2019). The weight is multiplied by the input of each neuron and added to bias to estimate the total output. Then, the error between observed and estimated outputs is measured. In the second step, the backward level starts to correct the weight values in the various connections so that the error between the estimated value and the observation is minimized (Moghaddam et al., 2019). Although BPA or other training methods of ANN are widely used, these training algorithms may fall into the trap of local optima or have slow convergence speed. Hence, the present study used optimization algorithms for training models to determine the weight and bias values.

2.2. ALO structure

ALO was inspired by the behaviour of ant lions in nature. Ant lions try to hunt ants. Therefore, they try to trap ants by creating pits (Mirjalili, 2015). The ant lions hide in the pits to hunt the ants trapped inside the pit. Ants move randomly in the search space based on equation (1):

$$x(t)=\left[0, cumsum\left(2r\left(t_1\right)-1\right), cumsumcumsum\left(2r\left(t_2\right)-1\right), .., cumsum\left(2r\left(t_n\right)-1\right)\right] \quad (1)$$

where cumsum: the cumulative sum, n: the maximum number of iterations, r: the random number, and $x(t)$: the random walk of ants.

The r value is calculated using equation (2):

$$r(t)=\begin{bmatrix}1 \leftarrow if\ (rand)>0.5\\ 0 \leftarrow if\ (rand \le 0.5)\end{bmatrix} \quad (2)$$

Equation (3) is used to make sure that ants do not move beyond the boundaries of the search space by a random step:

$$x_i^t=\frac{\left(x_i^t-a_i\right)\times d_i-c_i^t}{b_i-a_i}+c_i^t \quad (3)$$

where a_i: the minimum of random walk (RW) of the ith variable, b_i: the maximum of RW of the ith variable, c_i^t: the minimum of ith variable at ith iteration, and d_i: the maximum of ith variable at ith iteration

The ants use the roulette wheel in the next step. This cycle enables ALO to select ants with a better objective function. In the next step, the ant lions try to trap the ants by digging a pit. When the ants fall in a pit, the antlions prevent the ants from moving by throwing sand at the ants. Hence, the ant range of motion is reduced. Equations (4) and (5) simulate this behavior (Mirjalili, 2015).

$$c^t=\frac{c^t}{I} \quad (4)$$

$$d^t=\frac{d^t}{I} \quad (5)$$

where c^t : the minimum of all variables at tth iteration, d^t : the maximim of all variables at t th iteration, and I: a ration.

The random walk of ants is affected by antlions' traps. Thus, the position of the ant in the search space changes toward the antlion position. The parameters c and d are used to define the random walk of ants around the chosen antlion:

$$c_i^t = Antlion_j^t + c^t \tag{6}$$

$$d_i^t = Antlion_j^t + d^t \tag{7}$$

where $Antlion_j^t$: the location of chosen jth antlion at the tth iteration.

If the ants are fitter than its corresponding antlion, the antlion hunt ants. Thus, the antlions change their position according to the location of the hunted ant. Hence, the position of the ant lion is updated as follows (Mirjalili, 2015).

$$Antlion_j^t = Ant_i^t\,(if)\left(f\left(Ant_i^t\right) > f\left(Antlion_j^t\right)\right) \tag{8}$$

where Ant_i^t : the location of ith ant at the tth iteration, and f: the objective function.

The ALO uses the chosen antlion by the roulette wheel (ROW) and by the elite antlion to navigate the random walk of the ants. Figure 3 shows the steps of ALO optimization:

$$Ant_i^t = \frac{R_A^t + R_E^t}{2} \tag{9}$$

where R_A^t : the RW around the antlion chosen by the roulette wheel at the tth iteration, R_E^t : the RW around the elite antlion, and Ant_i^t : the location of the *ith* ant at the *tth* iteration.

2.3. Structure of bat algorithm

Bat Algorithm (BA) is considered as one of the optimization algorithms used in different fields, as shown in Table 1b. The bats use the echolocation ability to distinguish between obstacle and

food. To echolocate, the bats produce loud sounds. An echo is produced when sound hits the surroundings. Bats process the echo that comes back from obstacles. Each bat updates its sound frequency, position, and speed according to the following equations (Wang et al., 2019):

$$f_l = f_{\min} + \left(f_{\max} - f_{\min}\right) \times \vartheta \tag{10}$$

$$v_l\left(t\right) = \left(z_l\left(t\right) - z_*\right) \times f_i + v_l\left(t-1\right) \tag{11}$$

$$z_l\left(t\right) = z_l\left(t-1\right) + v_l\left(t\right) \tag{12}$$

where f_l: the frequency, $f_{\max}$: the maximum frequency, $f_{\min}$: the minimum frequency, ϑ: the random parameters, $z_l\left(t\right)$: the position of bats at iteration t, z_*: the best position of bats, $v_l\left(t-1\right)$: the velocity at iteration t-1, and $z_l\left(t-1\right)$: the position of bats at iteration t-1.

Bats use a random step operator to perform a local search. Moreover, the bats update their loudness and pulsation rate at each stage. Figure 4 shows the optimization steps based on BA:

$$z\left(t\right) = z\left(t-1\right) + \varepsilon A\left(t\right) \tag{13}$$

$$\begin{aligned} A_i^{t+1} &= \alpha A_i^t \\ r_i^t &= r_i^o \left[1 - \exp\left(-\gamma t\right)\right] \end{aligned} \tag{14}$$

where α: the constant value, γ: the constant value, r_i^t: the pulsation rate at iteration t, r_i^o: the initial value of pulsation rate, A_i^t: the loudness at iteration t, and A_i^{t+1}: the loudness at iteration t+1.

2.4. PSO

PSO algorithm is one of the most widely used algorithms for optimization in various fields, as shown in Table 1c. PSO is based on the social behavior of particles and the interaction of particles with each other. Each particle of PSO is considered as a candidate solution. Particles in PSO share their experiences. Each particle updates its speed and position based on the following

equation. First, the initial location of the particles is initialized. The value of fitness function for each particle is then determined. Finally, the speed and position of the particle are changed as follows

:.

$$v_i^{t+1} = wv_i^t + c_1 r_1 \left(x_{best} - x_i^t \right) + c_1 r_2 \left(x_{gbest} - x_i^t \right) \quad (15)$$

$$x_i^{t+1} = x_i^t + v_i^{t+1} \quad (16)$$

where x_{best}: the best particle position, x_{gbest}: the best group position, c_1 and c_2: the acceleration coefficients, w: the inertia weight, x_i^{t+1}: the position of particle at iteration t+1, v_i^{t+1}: the velocity of particle i at iteration t+1, r_1, and r_2: the random number.

3. Case study

The study predicts freshwater production in an Oman SSGH . The data were collected from Goosen et al. (2003). Goosen et al. (2003) focused on freshwater production and the effect of various parameters on the freshwater production. They predicted freshwater in the SSGH using a thermodynamic software based on mass transfer and heat transfer. The used software simultaneously required climate data, the length of the greenhouse, the width of the greenhouse, and other details to estimate the freshwater discharge.

As the available mathematical models need high computational time as well as a significant amount of data and details such as climate data, the current study used soft computing models to predict freshwater production, where 60 data were used as input data to the model. Input data to models were the height of the front evaporator, the length of the greenhouse, the width of the greenhouse, and roof transparency coefficient. To that end, 70% of the input data were used in the training phase and 30% in the testing phase. The produced freshwater was compared with the

actual values obtained from Goosen et al. (2003). Therefore, the soft computing models used in the study predicted freshwater production without using climatic data as well as solving complex mass-heat transfer equations. Table 2 shows the details of the input data used. The width of the greenhouse varied from 50 to 200 meters and the length of the greenhouse from 50 to 200 meters, an the transparency coefficient varied from 0.4 and 0.6 with the average transparency coefficient being 0.5 (table 3). Goosen et al. (2003) used 1995 meteorological data. Climatic data files included wind speed, relative humidity, wind direction, and temperature. In this study, the error indexes were used to evaluate the ability of models:

$$RMSE = \sqrt{\frac{\sum_{i=1}^{n}\left(WT_{ac} - WT_{es}\right)^2}{n}} \tag{17}$$

$$MAE = \frac{1}{n}\sum_{i=1}^{n}\left|WT_{ac} - WT_{es}\right| \tag{18}$$

$$PBIAS = 100 * \frac{\left[\sum_{i=1}^{n}\left(WT_{ac} - WT_{es}\right)^2\right]}{\sum_{i=1}^{n} WT_{ac}} \tag{19}$$

$$NSE = 1 - \frac{\left[\sum_{i=1}^{n}\left(WT_{ac} - WT_{es}\right)^2\right]}{\left[\sum_{i=1}^{n}\left(WT_{ac} - \overline{WT}_{ac}\right)^2\right]} \tag{20}$$

where $RMSE$: the root mean square error, MAE: the mean absolute error, $PBIAS$: the percent bias, NSE: the Nash-Sutcliff efficiency, WT_{ac}: the actual value of produced freshwater, WT_{es}: the estimated value of produced freshwater, and n: the number of data.

3.1. ANN hybrid models

283 The process of hybridizing ANN model starts with defining the training and testing data. Then
284 the training phase data was applied to determine the output of the training phase. If the
285 convergence criterion was satisfied, the models went to the test stage; otherwise, the ANN model
286 was connected to the optimization algorithm. First, at this step, the initial population of an
287 optimization algorithm was defined. Weight and bias were defined according to the initial
288 position of the bats, particles, and ant lions in the problem-solving space. The objective function
289 was then computed for each agent. The study used RMSE as the objective function. Operators of
290 various algorithms were then used to update the position of particles, bats, and ant lions.
291 Updating position means updating the initial values of weight and bias. Then, the used weight
292 and bias values were re-entered into the ANN model to run the model again for the training
293 phase. The study used the following indices to evaluate and correlate the models. Optimal
294 models had low RMSE, MAE, and PBIAS values with their NSE values high. Figure 5 shows
295 the time series of 60 data.

296 **3.2. Uncertainty analysis of models**

297 The model parameters and model inputs are considered as the sources of uncertainties. Thus, it
298 was essential to compute the uncertainty of models because of the uncertainty of model
299 parameters and model inputs. One of the most widely used methods to determine uncertainty is
300 the GLUE method which has been used to estimate the uncertainty of various hydraulic and
301 hydrological parameters (Ragab et al., 2020). The GLUE method was used based on the
302 following steps (Liu et al., 2020; Xu et al., 2020):

303 1- Prior probability parameter distribution (PPPD) was determined for each parameter. Two
304 scenarios were used in the study. The first scenario examined the uncertainty of the models due
305 to input data. The second scenario examined the uncertainty of models due to model parameters

like weight and bias that were obtained using optimization algorithms. The uncertainty of each scenario was separately calculated. Commonly, the normal distribution was chosen to calculate the PPPD of parameters. Although the normal or continuous distribution is used to obtain the prior distortion of the input data, these distributions, these distributions cannot be used for model parameters because the nature of the model parameters is not necessarily compatible with the normal or continuous distribution. However, the variability of the parameters during the training period can represent the properties of parameters. In this study, the calibrated 3000 ANN models were used to identify prior distributions of model parameters. The calibrated 3000 ANN models were enough because the parameter values were constant between 1000 to 3000 calibrated ANN models.

2. The Monte Carlo method was used to provide N samples of parameter sets from PPPD

3- ANN model was executed in each step, and the target outputs were calculated

4- The likelihood function was estimated according to the output values, and the actual output values. NSE was used as the objective function to calculate the likelihood function:

$$p\left(Y \mid \theta_i\right) = 1 - \frac{\sum_{n=1}^{N}\left[O_{obs} - O_{es}\right]^2}{\sum_{n=1}^{N}\left(O_{obs} - \bar{O}_{obs}\right)^2} \tag{21}$$

where $p\left(Y \mid \theta_i\right)$: the likelihood function, $\bar{O}_{obs}$: the mean observed value, O_{obs} : the observed value, and O_{es} : the estimated value.

5- A threshold was defined, so that those parameters that had a likelihood value below the threshold were not acceptable.

6- The posterior distribution density function was generated according to the following equation:

$$P(\theta_i \mid O) = \frac{P(\theta_i) * P(O \mid \theta_i)}{\sum_{i=1}^{N} P(O \mid \theta_i)} \quad (22)$$

Where $P(\theta_i \mid O)$: the posterior probability density, $P(\theta_i)$ the prior distribution, $P(O \mid \theta_i)$: Likelihood function

7- The mean value and standard variance of the estimated parameters were calculated as follows:

$$\mu(\theta) = \sum_{i=1}^{N} P(\theta_i \mid O) * \theta_i \quad (23)$$

$$\sigma(\theta) = \sum_{n=1}^{N} P(\theta_i \mid O) * (\theta_i - \mu) \quad (24)$$

where $\mu(\theta)$: the mean of the posterior distribution, $\sigma(\theta)$: the variance of the posterior distribution, and θ_i: the ith set parameter. In this study, the following indexes were used to measure the uncertainty of the models:

$$p - factor = \frac{NO_{in}}{N} \times 100 \quad (25)$$

$$r - Factor = \frac{\sum_{t=1}^{n} (GL_{t,u} - GL_{t,l})}{N\sigma_o} \quad (26)$$

Where, $p - factor$: 95% prediction uncertainty band (95PPU), NO_{in}: the number of observations enveloped by 95PPU, $GL_{t,u}$: the upper bound of variable, $GL_{t,l}$: the lower bound of variable, σ_o: the standard deviation of the observed, r: width of band and N: the number of observed data. The highest value of p and the lowest value of r show the best models.

4. Discussion and results

4.1. Sensitivity analysis of random parameters of optimization algorithms

Algorithms had random parameters whose exact value affected the accuracy and output of the algorithms. Thus, it was mandatory to determine the random parameters of optimization algorithms accurately. A sensitivity analysis means how different values of the random parameters affect the value of the objective function. Sensitivity analysis is used to study the effects of changes in the parameter of interest on the values of the objective function. While the parameter of interest is changed, the value of the other parameters is fixed. The optimal value of the parameter of interest minimizes the value of the objective function. For instance, Table 4 shows that ALO population size varied from 100 to 400. The best values of random parameters were obtained when the objective function reached its minimum value. In other words, when the error value reached its lowest value based on the objective function, the random parameter had the best value. Thus, the best value for ALO population size was 200 as the objective function was 0.545, which was the lowest value compared to other population sizes. Moreover, the best value for the maximum number of iterations of ALO was 100 as the lowest value of the objective function occurred at the maximum number of iterations of 100. Likewise, Table 4 shows the values of the random parameters of other algorithms.

4.2. Examining the effect of deleting various parameters on the accuracy of ANN-ALO model

Table 5 shows the effect of removing different parameters on the accuracy of ANN-ALO model. Results showed that the value of RMSE index when all input parameters were used was equal to 0.545 m^3 / day. The RMSE was increased from 0.545 m^3 / day to 0.964 m^3 by removing width from the input data. The highest decrease in NSE index occurred when the greenhouse width parameter was removed. Moreover, the highest increase in MAE and PBIAS indices occurred when the parameter width of the greenhouse was removed. A review of results showed that the

length of the greenhouse parameter was another key parameter in predicting freshwater production. The RMSE index was increased from 0.545 m^3 / day to 0.812 m^3 / day by removing the parameter of the length of the greenhouse. The study results showed that the parameters of the width and length of the greenhouse were the key parameters. Additionally, using four input combinations simultaneously dramatically increased the accuracy of models.

4.3. Comparing the performances of various models to predict freshwater production

Table 6 compares the performances of models in the training and testing phases. Results indicated that the RMSE value of ANN-ALO model was 0.545 m^3 / day, which was the lowest RMSE value in the training phase among the models. The RMSE value of ANN-ALO model was 17%, 36% and 40% lower than those of ANN-BA, ANN-PSO, and ANN models. Results also revealed that ANN-ALO model had the lowest MAE value.

Comparison of the performances of hybrid and ANN models indicated that the performance of the ANN model in the training stage was worse than those of other models. For instance, the ANN model PBIAS value in the training stage was 0.20, whereas the value of PBIAS index of ANN-BA, ANN-PSO, and ANN-ALO models was 0.14, 0.16, and 0.12, respectively. Comparison of models based on the NSE index showed that ANN-PSO model was weaker than other hybrid models like ANN-BA and ANN-ALO. Comparison of performances of the models in the test phase showed that the RMSE value of the ANN-ALO model was 18%, 33% and 39% lower than those of ANN-BA, ANN-PSO and ANN models. Furthermore, ANN-ALO model had the lowest MAE value among the models. The ANN model with 0.87 NSE value had the weakest performance among models. The ANN model had the highest PBIAS value among other models. Figure 6 shows the scatterplots for various models. All data were used as input data to extract R^2 coefficients. Outputs showed that the ANN-ALO model had the highest R^2 coefficient among

models. Furthermore, results showed that ANN model had the lowest R^2 coefficient. Figure 7 shows a box plot for different models. Results showed that the output of ANN-ALO model was more compatible with the actual outputs than other models. Figures 8 and 9 indicate the uncertainty of models used in the first and second scenarios. As can be seen in figure 8, the ANN-ALO provided the lowest uncertainty with p: 0.97 and r: 0.21 in the first scenario. The highest uncertainty was obtained for the ANN model with p:0.90 and r:0.27. However, the results show that the integration of models and optimization algorithms decreased uncertainty. As can be seen in figure 9, the ANN-ALO provided the lowest p (p:0.94) and the highest r (0.23). The results indicated that the standalone ANN model had higher uncertainty than those of the hybrid ANN models.

Moreover, comparison of the uncertainty of models in both scenarios indicated that the uncertainty of models was higher in the second scenario, showing that the model parameters caused more uncertainty in comparison to the input parameters. Taylor diagram shows the model with the best performance according to the correlation coefficient, standard deviation and RMSE index. Figure 10 shows the Taylor diagram. The Taylor diagram is based on the total input data. Simulated patterns that match well with measured data will place nearest the reference point on the x-axis. The results showed that ANN-ALO had better performance compared to other models. Nonetheless, the results indicated that the ANN model had weaker performance compared to other models.

4.4. Examining the effect of various input parameters on freshwater production

This section examines the effect of changing the values of input parameters on the freshwater production. Figure 11 shows the effect of changing the width of the greenhouse at various lengths on freshwater production. The height of evaporator for all cases of Figure 11 was 2 meters, and the transparency coefficient was 0.4. Results indicated that the freshwater production

414 increased with an increase in the width at the fixed length of 50 meters. With an increase in
415 width from 50 meters to 200 meters, the value of produced freshwater increased from $5m^3$ / day
416 to $90m^3$ / day at the length of 50 meters. With an increase in width from 50 meters to 200 meters,
417 the produced freshwater increased from $32m^3$ / day to $138m^3$ / day at the length of 100 meters.
418 The value of produced freshwater decreased at a constant length of 200 meters when the
419 greenhouse width increased from 150 to 200. Larger greenhouse widths increase the contact area
420 between air and saltwater in the evaporator. Thus, the width of the greenhouse is a key parameter
421 for producing fresh water production
422 Figure 12 shows the change in greenhouse width at different lengths of the greenhouse for a roof
423 transparency coefficient of 0.4 and an evaporator height of 3 m. The freshwater produced during
424 the first 200 meters had a downward trend and then had an upward trend. The lowest value of
425 freshwater produced occurred within 200 m length at 100 m width. Additionally, the freshwater
426 produced during the first 150 meters had a downward trend and then had an upward trend.
427 Likewise, the freshwater produced in lengths of 100 and 50 meters for different widths first had a
428 downward trend and then had an upward one. Zarei and Behyad (2019) reported that the
429 freshwater produced for the case study of the present study increased at an evaporator height of 2
430 m and a roof transparency coefficient of 0.4 with increasing width at all lengths except 200 m.
431 Additionally, they stated that the water produced for a height of 3 meters first had a downward
432 trend and then an upward one. Thus, their findings confirm the results of the present study.
433 Figure 13 shows the effect of height change at various widths on the value of freshwater
434 produced. The length of the greenhouse was equal to 200 meters, and the transparency
435 coefficient was 0.4 for all cases. Results revealed that the height of 2 meters produced the highest
436 freshwater for various widths except for 200 meters. The lowest value of the water produced for

different widths occurred at a height of 3 m. However, the increase in the height of the evaporator did not increase the production of freshwater, as the air distribution did not happen well at higher heights.

5. Conclusion

Freshwater production is of great significance given the increase in demand, particularly in the agricultural irrigation sector. The study examined the prediction of freshwater production in an SSGH using ANN hybrid models. The greenhouse length, width, roof transparency coefficient and front evaporator height were used as model input. Examining the input parameters revealed that the greenhouse width was the most critical parameter among all input parameters. Moreover, using 4 input parameters simultaneously increased the accuracy of models. Comparison of performance of models showed that the ANN-ALO model had the lowest RMSE value at the training and testing levels. The outputs of models showed that the RMSE value of the ANN-ALO model was 0.545 m3 / day. The MAE values of ANN-BA, ANN-PSO, and ANN models in the testing phase were 0.612m3 / day, 0.823m^3 / day, and 0.901m^3 / day, respectively. Results indicated that the lowest value of NSE index and the highest value of PBIAS index in training and testing were obtained by ANN. Also, the uncertainty of predictive models was considered for two scenarios: (1) uncertainty of input and (2) uncertainty of model parameters. The performance of models revealed that the uncertainty of ANN-ALO was lower than those of the other models in both scenarios. Further, the uncertainty of hybrid and standalone ANN models was higher in the second scenario, showing that the model parameters caused more uncertainty than did the input parameters. The effect of varying parameters on freshwater production was also evaluated. Results indicated that freshwater production in the greenhouse with an evaporator height of 2 m and a roof transparency coefficient of 0.4 increased with the increase in width at a

460 fixed length of 50 m. Additionally, the freshwater production increased with the increase in
461 width along 100 meters. However, future researches can examine the effect of other inputs such
462 as climatic parameters on the freshwater production. Also, to ensure the performance of soft
463 calculation methods, freshwater production can be predicted for greenhouses located in different
464 climates using climatic data.

465

466 # Refrences

467 Abualigah, L., & Diabat, A. (2020). A novel hybrid antlion optimization algorithm for multi-
468 objective task scheduling problems in cloud computing environments. Cluster Computing, 1-19.
469 Al-Khalidi, A. A. T., Zurigat, Y. H., Dawoud, B., Aldoss, T., & Theodoridis, G. (2010, March).
470 Performance of a greenhouse deslaination condenser: An experimental study. In 2010 1st
471 International Nuclear & Renewable Energy Conference (INREC) (pp. 1-7). IEEE.

472

473 Al-Ismaili, A. M., Jayasuriya, H., Al-Mulla, Y., & Kotagama, H. (2018). Empirical model for the
474 condenser of the seawater greenhouse. *Chemical Engineering Communications*, *205*(9), 1252-
475 1260.
476 Al-Ismaili, A. M., Ramli, N. M., Azlan Hussain, M., & Rahman, M. S. (2019). Artificial neural
477 network simulation of the condenser of seawater greenhouse in Oman. *Chemical Engineering*
478 *Communications*, *206*(8), 967-985.
479 Apornak, A., Raissi, S., Keramati, A., & Khalili-Damghani, K. (2020). Optimizing human
480 resource cost of an emergency hospital using multi-objective Bat algorithm. International Journal
481 of Healthcare Management, 1-7.

Ang, K. M., Lim, W. H., Isa, N. A. M., Tiang, S. S., & Wong, C. H. (2020). A constrained multi-swarm particle swarm optimization without velocity for constrained optimization problems. *Expert Systems with Applications*, *140*, 112882.

Bi, J., Yuan, H., Duanmu, S., Zhou, M. C., & Abusorrah, A. (2020). Energy-optimized Partial Computation Offloading in Mobile Edge Computing with Genetic Simulated-annealing-based Particle Swarm Optimization. IEEE Internet of Things Journal.

Bui, D. T., Hoang, N. D., Nguyen, H., & Tran, X. L. (2019). Spatial prediction of shallow landslide using Bat algorithm optimized machine learning approach: A case study in Lang Son Province, Vietnam. *Advanced Engineering Informatics*, *42*, 100978.

Cai, X., Zhang, J., Liang, H., Wang, L., & Wu, Q. (2019). An ensemble bat algorithm for large-scale optimization. International Journal of Machine Learning and Cybernetics, 10(11), 3099-3113.

Chen, X., Li, K., Xu, B., & Yang, Z. (2020). Biogeography-based learning particle swarm optimization for combined heat and power economic dispatch problem. Knowledge-Based Systems, 208, 106463.

Chen, K., Zhou, F. Y., & Yuan, X. F. (2019). Hybrid particle swarm optimization with spiral-shaped mechanism for feature selection. Expert Systems with Applications, 128, 140-156.

Cui, Z., Zhang, J., Wu, D., Cai, X., Wang, H., Zhang, W., & Chen, J. (2020). Hybrid many-objective particle swarm optimization algorithm for green coal production problem. Information Sciences, 518, 256-271.

504 Deotti, L. M. P., Pereira, J. L. R., & da Silva Júnior, I. C. (2020). Parameter extraction of
505 photovoltaic models using an enhanced Lévy flight bat algorithm. Energy Conversion and
506 Management, 221, 113114.
507 Dhal, K. G., & Das, S. (2020). Local search-based dynamically adapted bat algorithm in image
508 enhancement domain. International Journal of Computing Science and Mathematics, 11(1), 1-28.
509 Essa, F. A., Abd Elaziz, M., & Elsheikh, A. H. (2020). Prediction of power consumption and
510 water productivity of seawater greenhouse system using random vector functional link network
511 integrated with artificial ecosystem-based optimization. *Process Safety and Environmental*
512 *Protection*, *144*, 322-329.
513 Farshi, T. R., Drake, J. H., & Özcan, E. (2020). A multimodal particle swarm optimization-based
514 approach for image segmentation. Expert Systems with Applications, 149, 113233.
515 Ghimire, S., Deo, R. C., Downs, N. J., & Raj, N. (2019). Global solar radiation prediction by
516 ANN integrated with European Centre for medium range weather forecast fields in solar rich
517 cities of Queensland Australia. *Journal of cleaner production*, *216*, 288-310.
518 Goosen, M. F. A., Sablani, S. S., Paton, C., Perret, J., Al-Nuaimi, A., Haffar, I., ... & Shayya, W.
519 H. (2003). Solar energy desalination for arid coastal regions: development of a humidification–
520 dehumidification seawater greenhouse. *Solar energy*, *75*(5), 413-419.
521 Hong, W. C., Li, M. W., Geng, J., & Zhang, Y. (2019). Novel chaotic bat algorithm for
522 forecasting complex motion of floating platforms. Applied Mathematical Modelling, 72, 425-
523 443.
524 Hu, Y., Zhang, Y., & Gong, D. (2020). Multiobjective particle swarm optimization for feature
525 selection with fuzzy cost. IEEE Transactions on Cybernetics.

526 Jahani, B., & Mohammadi, B. (2019). A comparison between the application of empirical and
527 ANN methods for estimation of daily global solar radiation in Iran. *Theoretical and Applied*
528 *Climatology*, *137*(1-2), 1257-1269.
529 Junior, F. E. F., & Yen, G. G. (2019). Particle swarm optimization of deep neural networks
530 architectures for image classification. *Swarm and Evolutionary Computation*, *49*, 62-74.
531 Kumar, S., Roshni, T., & Himayoun, D. (2019). A comparison of emotional neural network
532 (ENN) and artificial neural network (ANN) approach for rainfall-runoff modelling. *Civil*
533 *Engineering Journal*, *5*(10), 2120-2130.
534 Li, Y., Wei, K., Yang, W., & Wang, Q. (2020). Improving wind turbine blade based on multi-
535 objective particle swarm optimization. *Renewable Energy*, *161*, 525-542.
536 Liu, L., Luo, S., Guo, F., & Tan, S. (2020). Multi-point shortest path planning based on an
537 Improved Discrete Bat Algorithm. *Applied Soft Computing*, *95*, 106498.
538 Liu, J., Shao, W., Xiang, C., Mei, C., & Li, Z. (2020). Uncertainties of urban flood modeling:
539 Influence of parameters for different underlying surfaces. *Environmental Research*, *182*, 108929.
540 Mahmoudi, H., Spahis, N., Abdul-Wahab, S. A., Sablani, S. S., & Goosen, M. F. (2010).
541 Improving the performance of a Seawater Greenhouse desalination system by assessment of
542 simulation models for different condensers. *Renewable and Sustainable Energy Reviews*, *14*(8),
543 2182-2188.
544 Malik, A., Kumar, A., Kim, S., Kashani, M. H., Karimi, V., Sharafati, A., ... & Chau, K. W.
545 (2020). Modeling monthly pan evaporation process over the Indian central Himalayas:
546 application of multiple learning artificial intelligence model. *Engineering Applications of*
547 *Computational Fluid Mechanics*, *14*(1), 323-338.

548 Mirarabi, A., Nassery, H. R., Nakhaei, M., Adamowski, J., Akbarzadeh, A. H., & Alijani, F.
549 (2019). Evaluation of data-driven models (SVR and ANN) for groundwater-level prediction in
550 confined and unconfined systems. Environmental Earth Sciences, 78(15), 489.
551 Mirjalili, S. (2015). The ant lion optimizer. Advances in engineering software, 83, 80-98.
552 Moghaddam, H. K., Moghaddam, H. K., Kivi, Z. R., Bahreinimotlagh, M., & Alizadeh, M. J.
553 (2019). Developing comparative mathematic models, BN and ANN for forecasting of
554 groundwater levels. *Groundwater for Sustainable Development*, *9*, 100237.
555 Niu, W. J., Feng, Z. K., Chen, Y. B., Min, Y. W., Liu, S., & Li, B. J. (2020). Multireservoir
556 system operation optimization by hybrid quantum-behaved particle swarm optimization and
557 heuristic constraint handling technique. Journal of Hydrology, 590, 125477.
558 Notton, G., Voyant, C., Fouilloy, A., Duchaud, J. L., & Nivet, M. L. (2019). Some applications
559 of ANN to solar radiation estimation and forecasting for energy applications. *Applied Sciences*,
560 *9*(1), 209.
561 Oliva, D., Hinojosa, S., Abd Elaziz, M., & Ortega-Sánchez, N. (2018). Context based image
562 segmentation using antlion optimization and sine cosine algorithm. Multimedia Tools and
563 Applications, 77(19), 25761-25797.
564 Pan, J. S., & Dao, T. K. (2019). A compact bat algorithm for unequal clustering in wireless
565 sensor networks. Applied Sciences, 9(10), 1973.
566 Qasem, S. N., Samadianfard, S., Kheshtgar, S., Jarhan, S., Kisi, O., Shamshirband, S., & Chau,
567 K. W. (2019). Modeling monthly pan evaporation using wavelet support vector regression and
568 wavelet artificial neural networks in arid and humid climates. *Engineering Applications of*
569 *Computational Fluid Mechanics*, *13*(1), 177-187.

570 Ragab, R., Kaelin, A., Afzal, M., & Panagea, I. (2020). Application of Generalized Likelihood
571 Uncertainty Estimation (GLUE) at different temporal scales to reduce the uncertainty level in
572 modelled river flows. *Hydrological Sciences Journal*, (just-accepted).
573 Rani, R. R., & Ramyachitra, D. (2020). Antlion optimization algorithm for pairwise structural
574 alignment with bi-objective functions. Neural Computing and Applications, 32(11), 7079-7096
575 Samantaray, S., Tripathy, O., Sahoo, A., & Ghose, D. K. (2020). Rainfall Forecasting Through
576 ANN and SVM in Bolangir Watershed, India. In *Smart Intelligent Computing and Applications*
577 (pp. 767-774). Springer, Singapore.
578 Sadeghi, D., Naghshbandy, A. H., & Bahramara, S. (2020). Optimal sizing of hybrid renewable
579 energy systems in presence of electric vehicles using multi-objective particle swarm
580 optimization. *Energy*, *209*, 118471.
581 Sangaiah, A. K., Sadeghilalimi, M., Hosseinabadi, A. A. R., & Zhang, W. (2019). Energy
582 consumption in point-coverage wireless sensor networks via bat algorithm. *IEEE Access*, *7*,
583 180258-180269.
584 Sharghi, E., Nourani, V., Molajou, A., & Najafi, H. (2019). Conjunction of emotional ANN
585 (EANN) and wavelet transform for rainfall-runoff modeling. *Journal of Hydroinformatics*, *21*(1),
586 136-152.
587 Singh, A., Singh, R. M., Kumar, A. R., Kumar, A., Hanwat, S., & Tripathi, V. K. (2019).
588 Evaluation of soft computing and regression-based techniques for the estimation of evaporation.
589 *Journal of Water and Climate Change*.
590 Talbi, N. (2019). Design of fuzzy controller rule base using bat algorithm. *Energy Procedia*, *162*,
591 241-250.

592 Tahri, T., Abdul-Wahab, S., Bettahar, A., Douani, M., Al-Hinai, H., & Al-Mulla, Y. (2009).
593 Simulation of the condenser of the seawater greenhouse: Part I: Theoretical development.
594 Journal of thermal analysis and calorimetry, 96(1), 35-42.
595 Tahri, T., Douani, M., Amoura, M., & Bettahar, A. (2016). Study of influence of operational
596 parameters on the mass condensate flux in the condenser of seawater greenhouse at Muscat,
597 Oman. Desalination and Water Treatment, 57(30), 13930-13937.
598
599 Tharwat, A., & Hassanien, A. E. (2018). Chaotic antlion algorithm for parameter optimization of
600 support vector machine. Applied Intelligence, 48(3), 670-686.
601 Tian, D., Zhao, X., & Shi, Z. (2019). Chaotic particle swarm optimization with sigmoid-based
602 acceleration coefficients for numerical function optimization. Swarm and Evolutionary
603 Computation, 51, 100573.
604 *Tiwari, S., Vaddi, N., Metta, S. B., & Kumar, M. (2020, April). Optimal Power Flow Solution*
605 *with Nature Inspired Antlion Meta-Heuristic Algorithm. In Journal of Physics: Conference*
606 *Series (Vol. 1478, No. 1, p. 012035). IOP Publishing.*
607 Yue, X., & Zhang, H. (2020). Modified hybrid bat algorithm with genetic crossover operation
608 and smart inertia weight for multilevel image segmentation. Applied Soft Computing, 90,
609 106157.
610 Van, T. P., Snášel, V., & Nguyen, T. T. (2020). Antlion optimization algorithm for optimal non-
611 smooth economic load dispatch. International Journal of Electrical & Computer Engineering
612 (2088-8708), 10.
613 Wang, Y., Wang, P., Zhang, J., Cui, Z., Cai, X., Zhang, W., & Chen, J. (2019). A novel bat
614 algorithm with multiple strategies coupling for numerical optimization. *Mathematics*, *7*(2), 135.

615 Xu, H., Ma, C., Xu, K., Lian, J., & Long, Y. (2020). Staged optimization of urban drainage
616 systems considering climate change and hydrological model uncertainty. *Journal of Hydrology*,
617 124959.
618
619 Yadav, B., Gupta, P. K., Patidar, N., & Himanshu, S. K. (2020). Ensemble modelling framework
620 for groundwater level prediction in urban areas of India. Science of The Total Environment, 712,
621 135539.
622
623 Yetilmezsoy, K., & Abdul-Wahab, S. A. (2014). A composite desirability function-based
624 modeling approach in predicting mass condensate flux of condenser in seawater greenhouse.
625 *Desalination*, *344*, 171-180.
626 Zarei, T., Behyad, R., & Abedini, E. (2018). Study on parameters effective on the performance
627 of a humidification-dehumidification seawater greenhouse using support vector regression.
628 *Desalination*, *435*, 235-245.
629 Zarei, T., & Behyad, R. (2019). Predicting the water production of a solar seawater greenhouse
630 desalination unit using multi-layer perceptron model. *Solar Energy*, *177*, 595-603.
631 Zeng, X., Wang, W., Chen, C., & Yen, G. G. (2019). A consensus community-based particle
632 swarm optimization for dynamic community detection. IEEE Transactions on Cybernetics,
633 50(6), 2502-2513.
634 Zhang, X., Liu, H., & Tu, L. (2020). A modified particle swarm optimization for multimodal
635 multi-objective optimization. *Engineering Applications of Artificial Intelligence*, *95*, 103905.
636
637

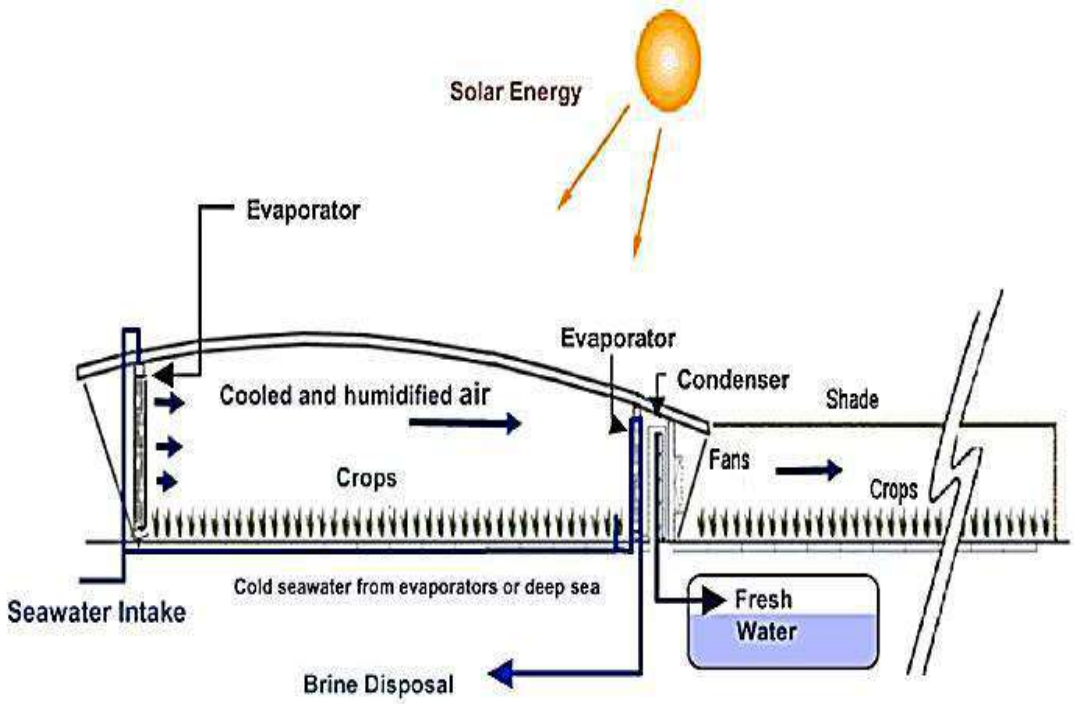

Figure 1. Strcture of a seawater greenhouse (Goosen et al., 2003)

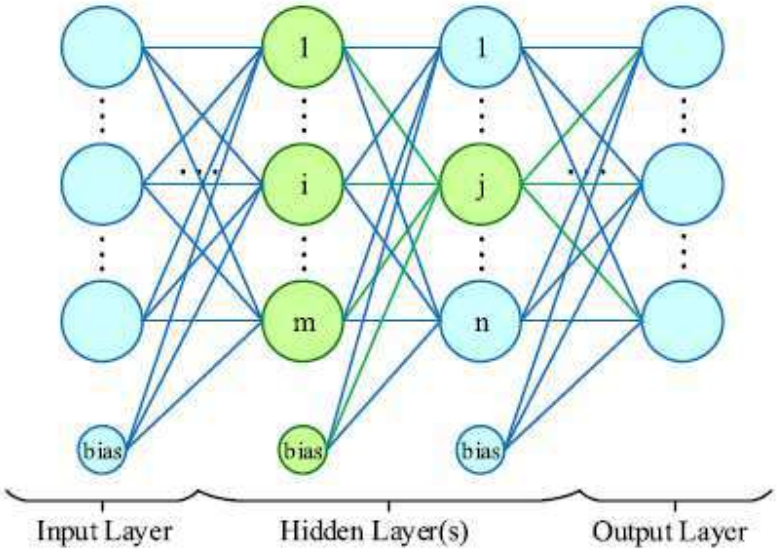

645

$$O_k = f_o\left[\sum_{i=1}^{M_n} \omega_{kj} \times f_h\left(\sum_{i=1}^{N} \omega_{ji} x_i + b_{jo}\right) + b_{ko}\right]$$

Where, f_o:the activation function of the output neuron, f_h:the activation function of the hidden neuron, x_i: the input data, i: input neuron, j: hidden neuron, k: output neuron, ω_{kj}: weight in the output layer linking the jth neuron in the middle layer and the kth neuron in the last layer, ω_{ji}: weight in the hidden layer connecting the ith neuron in the input layer and the jth neuron in the hidden layer b_{jo} is the bias for the jth hidden neuron, b_{ko} is the bias for the kth output neuron, M_n: number of hidden neurons, and N_n: Number of input

646

647

648 Figure 2. The stcrture of MLP model

649 Table 1. Literature review of applications of a: ALO, b: BA, and c: PSO

650 (a)

651

Author	Filed
Abualigah and Diabat (2020)	multi-objective task scheduling problems in cloud computing environments
Van et al. (2020)	Optimal non-smooth economic load dispatch.
Rani and Ramyachitra (2020)	Pairwise structural alignment with bi-objective functions
Tiwari et al. (2020)	Optimal Power Flow Solution
Tharwat and Hassanien (2018)	Parameter optimization of support vector machine
Oliva et al. (2018)	Context based image segmentation
Mahanta et al. (2020)	The optimal design of the robotic gripper

652 653 654 655 656 657 658 659 660 661 662 663 664 665 666 667 668 669 670 671 672 673

674 b

675

Author	Filed	Author	Filed
Liu et al. (2020)	Multi-point shortest path planning	Gupta et al. (2019)	Classification of white blood cells
Deotti et al. (2020)	Parameter extraction of photovoltaic models	Dhal and Das (2020)	Image enhancement domain
Cai et al. (2019)	Large-scale optimization	Bui et al. (2019)	Spatial prediction of shallow landslide
Wang et al. (2019)	Numerical optimization	Bento et al. (2019)	Optimization of neural network
Hong et al. (2019)	Forecasting complex motion of floating platforms	Yue and Zhang (2020)	multilevel image segmentation
Sangaiah et al. (2019)	Energy consumption in point-coverage wireless sensor networks	Apornak et al. (2020)	Optimizing human resource cost of an emergency hospital
Pan and Dao (2019)	unequal clustering in wireless sensor networks	Talbi (2019)	Design of fuzzy controller rule base

676

677

678

679

680

681

c

Author	Filed	Author	Filed
Junior and Yen (2019)	Image classification	Hu et al. (2020)	Feature selection with fuzzy cost
Zeng et al. (2019)	Dynamic community detection	Chen et al. (2020)	Power economic dispatch problem
Niu et al. (2020)	Multireservoir system operation optimization	Ang et al. (2020)	Constrained optimization problems
Chen et al. (2019)	Feature selection	Sadeghi et al. (2020)	Optimal sizing of hybrid renewable energy systems
Cui et al. (2020)	Green coal production problem	Farshi et al. (2020)	image segmentation
Tian et al. (2019)	Numerical function optimization	Li et al. (2020)	Improving wind turbine blade
Zhang et al. (2020)	multimodal multi-objective optimization	Bi et al. (2020)	Energy-optimized Partial Computation Offloading in Mobile Edge Computing

Initialize the first population of ants and antlions randomly
Calculate the fitness of ants and antlions
Find the best ant lions and assume it as the elite (determined optimum)
While the end criterion is not satisfied
For every ant
Select an ant lion using Roulette wheel
Update c and d using equations Eqs. (4) and (5)
Create a random walk and normalize it using Eqs. (1) And
(3)
Update the position of ant using (9)
End for
Calculate the fitness of all ants
Replace an ant lion with its corresponding ant it if becomes
Fitter (Eq. (8))
Update elite if an ant lion becomes fitter than the elite
End while
Return elite

Figure 3. The pseudo code of ALO

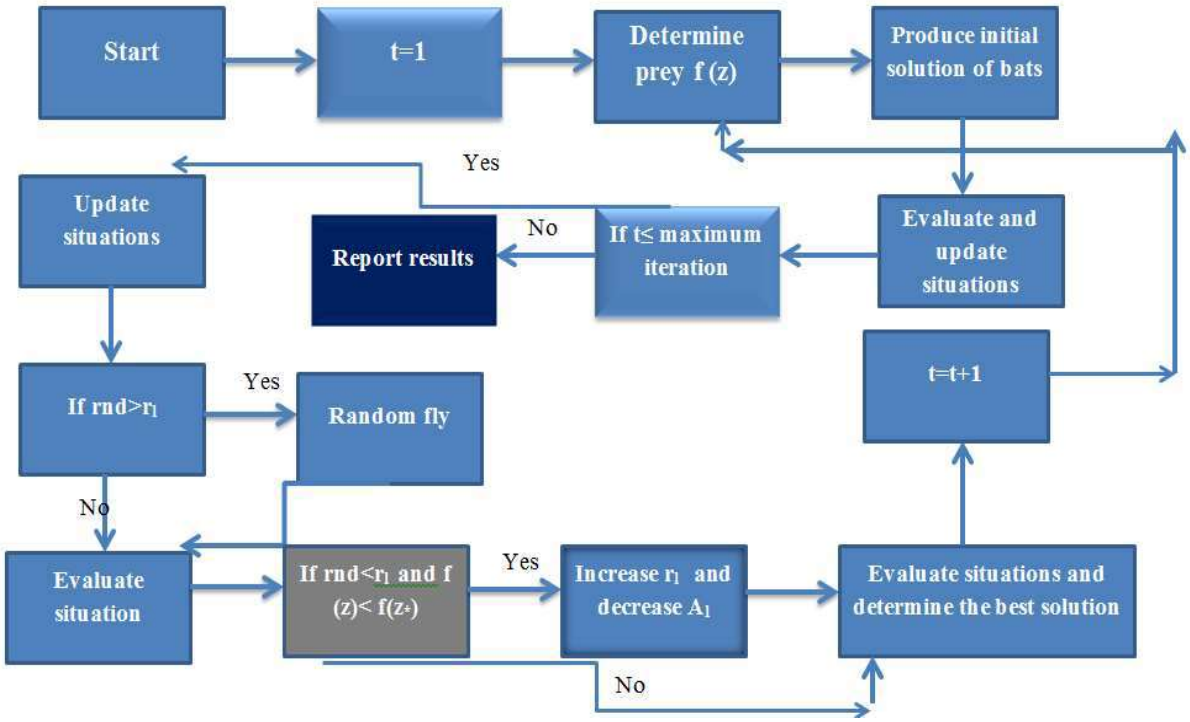

Figure 4. Flowchart of BA

Table 2. Ranges of parameters in the seawater greenhouse

Parameter	Ranges of changes	Mean value of the parameter	Standard deviation
Width	50-200 (m)	110.114	45.97
Length	50-200 (m)	110.114	45.97
Height of the front evaporator	2-4 (m)	3m	0.81
Roof transparency	0.40-0.60 (m)	0.50	0.10

Table 3. Values of constant parameters in the seawater greenhouse

Parameter	Ranges of changes
Height of the planting area	4m
Height of the rear evaporator	2m
Height of the condenser	2m
Greenhouse orientation	40° N
Flow rate	$0.1m^3/s$
Fin spacing	0.0025m
Air flow changes	0.15 l/min

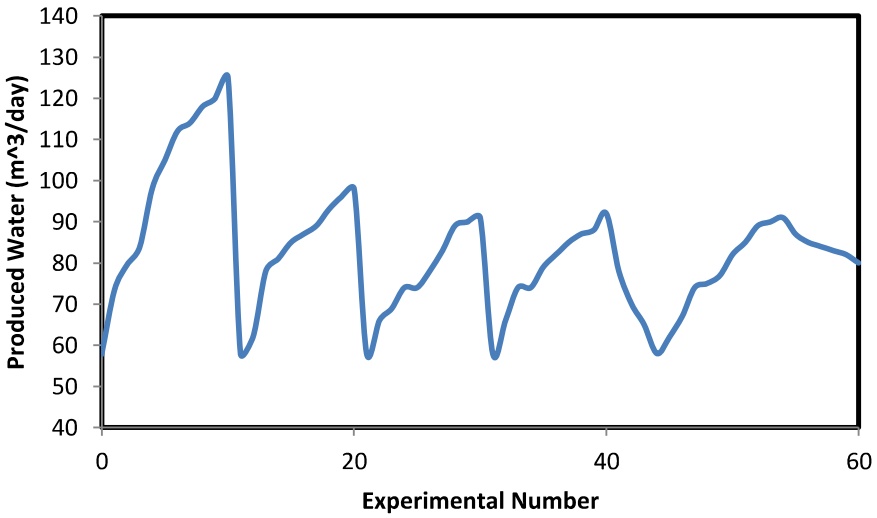

Figure 5. The time series of produced water

Table 4. Sensitivity Analysis for random parameters for a: ALO, b: PSO, and c: BA

a

Population size	Objective Function	Maximum number of Iterations	Objective Function
100	0.654	50	0.698
200	0.545	100	0.544
300	0.712	150	0.712
400	0.823	200	0.802

b

Population size	Objective Function	Maximum number of Iterations	Objective Function	$c_1=c_2$	Objective Function	w	Objective Function
100	0.923	50	0.967	1.60	0.989	0.30	0.989
200	0.845	100	0.912	1.80	0.895	0.50	0.845
300	0.934	150	0.845	2.0	0.845	0.70	0.897
400	1.02	200	0.898	2.2	0.899	0.90	0.934

C (OF: objective function, MIF: minimum frequency, MIL: minimum loudness, MAL: maximum loudness, and MAF: maximum frequency)

Population size	OF	MAF	OF	MIF	OF	MAL	OF	MIL	OF	Maximum number of Iterations	OF
100	0.712	3	0.724	1	0.684	0.3	0.712	0.10	0.714	50	0.699
200	0.655	5	0.689	2	0.655	0.50	0.655	0.20	0.712	100	0.655
300	0.689	7	0.655	3	0.698	0.70	0.724	0.30	0.655	150	0.712
400	0.912	9	0.845	4	0.712	0.90	0.872	0.40	0.698	200	0.745

717 Table 5. Effect of elimination of different parameters on the accuracy of ANN-ALO

718

Inputs	RMSE	MAE	NSE	PBIAS
Length of greenhouse, width of greenhouse, height of the front evaporator, roof transparency	0.545	0.456	0.96	0.12
Length of greenhouse, roof transparency , and height of the front evaporator	0. 964	0.868	0.90	0.29
width of greenhouse, Length of greenhouse, roof transparency	0.723	0.689	0.94	0.15
Length of greenhouse, height of the front evaporator, width of greenhouse	0.729	0.694	0.92	0.16
width of greenhouse, height of the front and, roof transparency	0.812	0.745	0.91	0.22

719

720

721 **Table 6.** Comparison of performances of different models based on statistical indexes

Model	RMSE	MAE	NSE	PBIAS
ANN-ALO	0.545	0.456	0.96	0.12
ANN-BA	0.655	0.567	0.95	0.14
ANN-PSO	0.846	0.672	0.92	0.16
ANN	0.912	0.714	0.90	0.20
ANN-ALO	0.612	0.545	0.94	0.16
ANN-BA	0.745	0.612	0.90	0.18
ANN-PSO	0.912	0.823	0.89	0.20
ANN	0.998	0.901	0.87	0.22

722

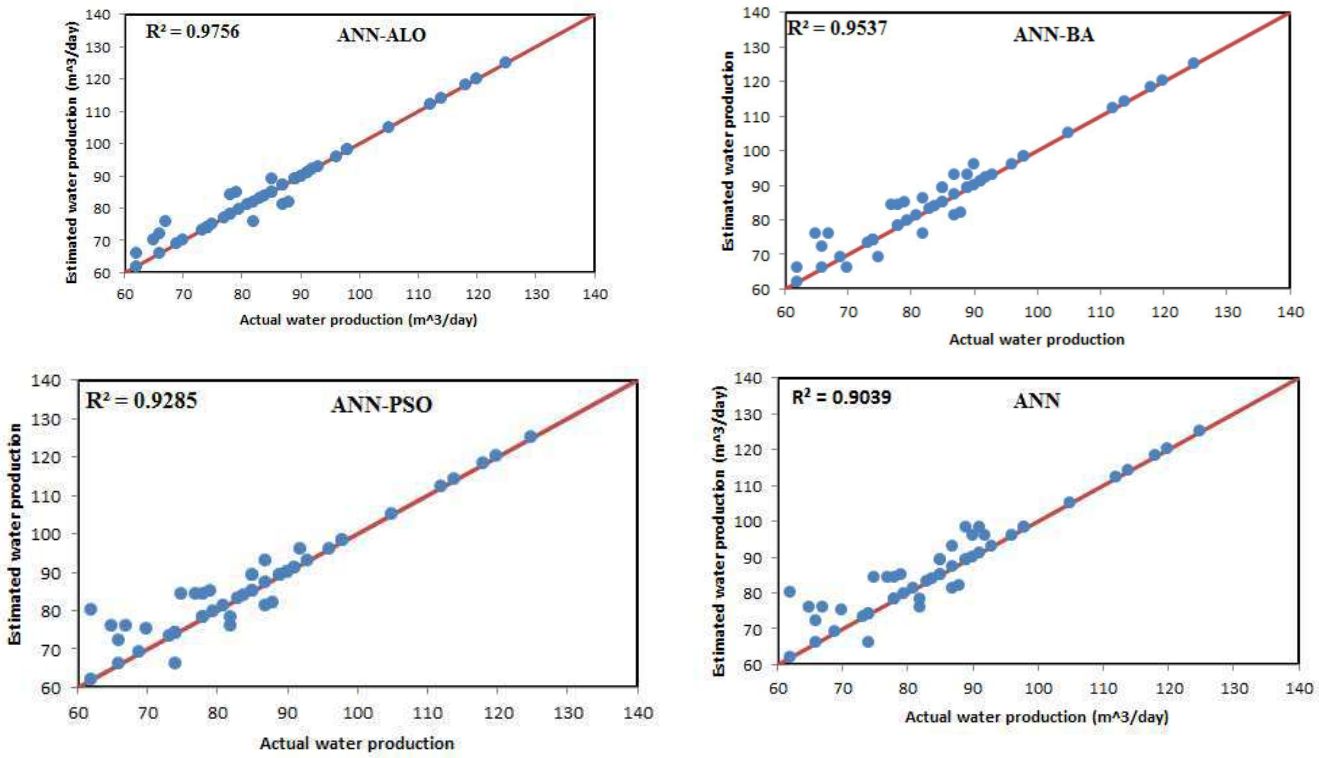

723

724

725 Figure 6. The scatter plots for the models

726

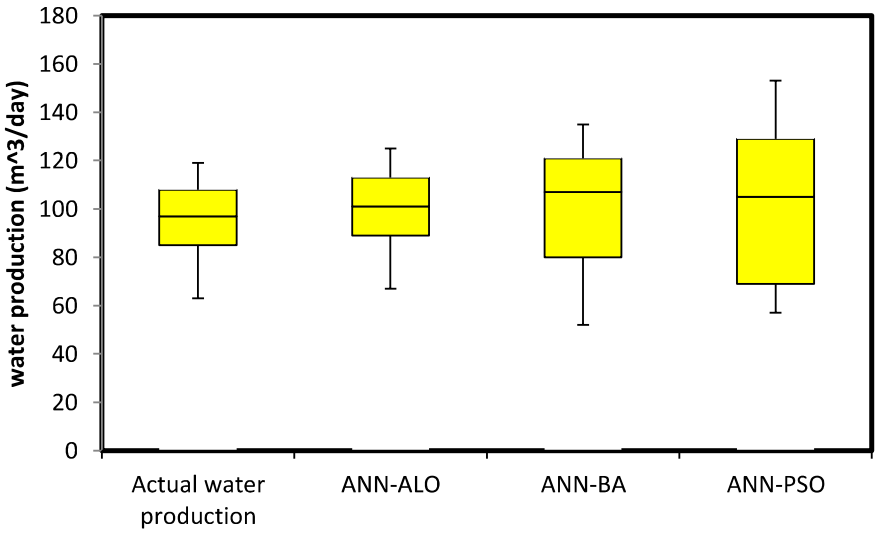

727

728

729 Figure 7. Boxplot of different models

730

731

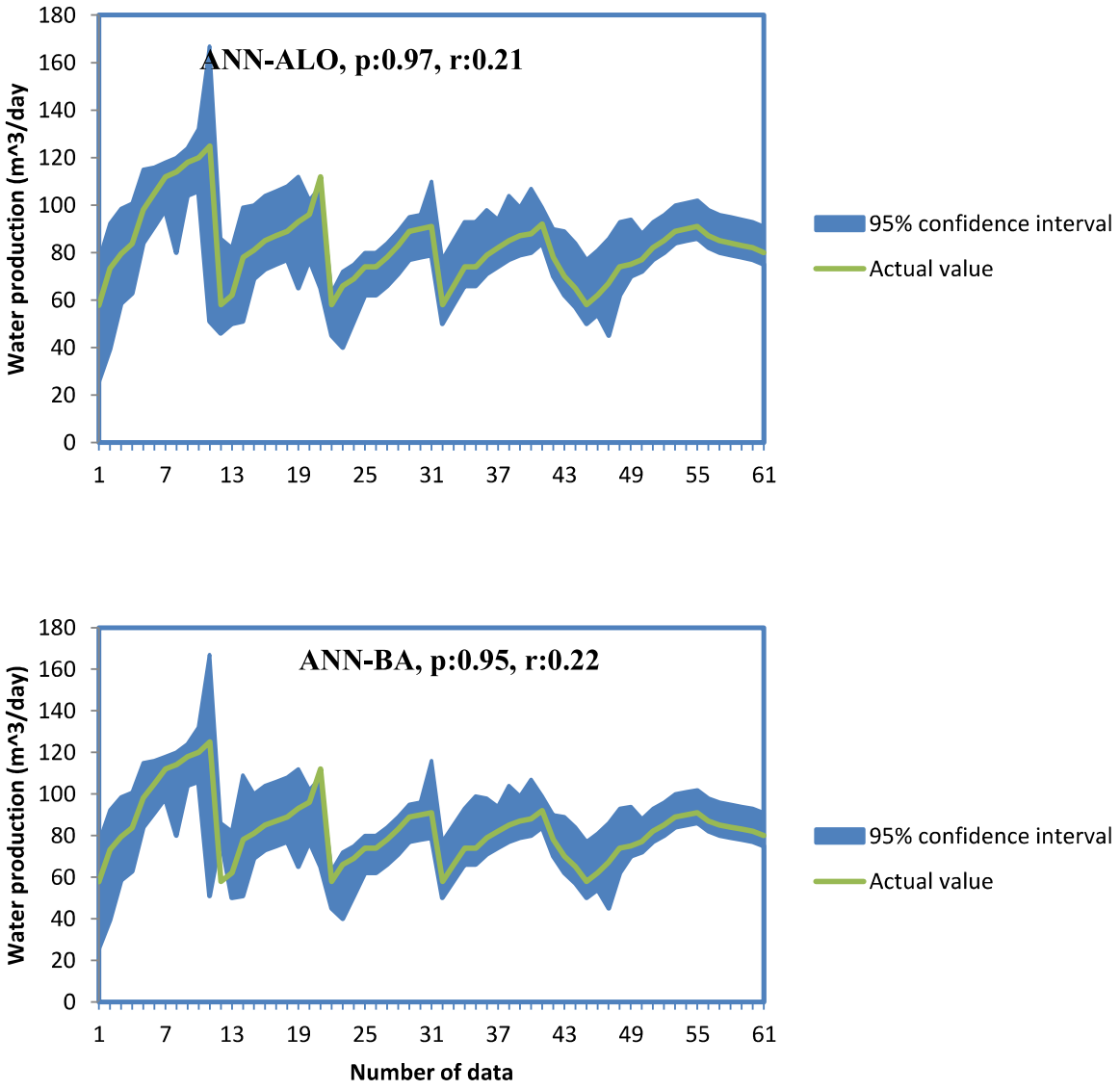

732

733

734

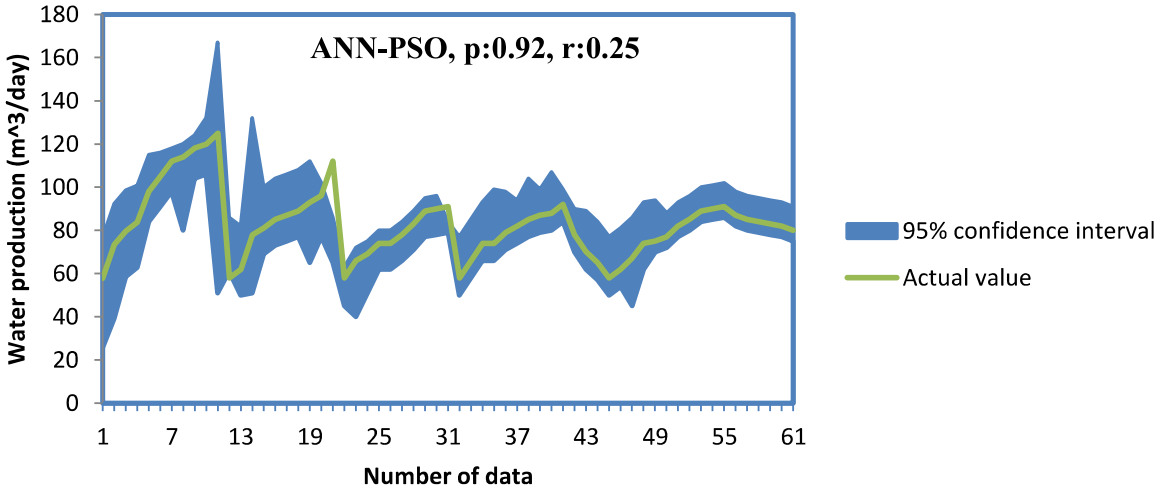

735

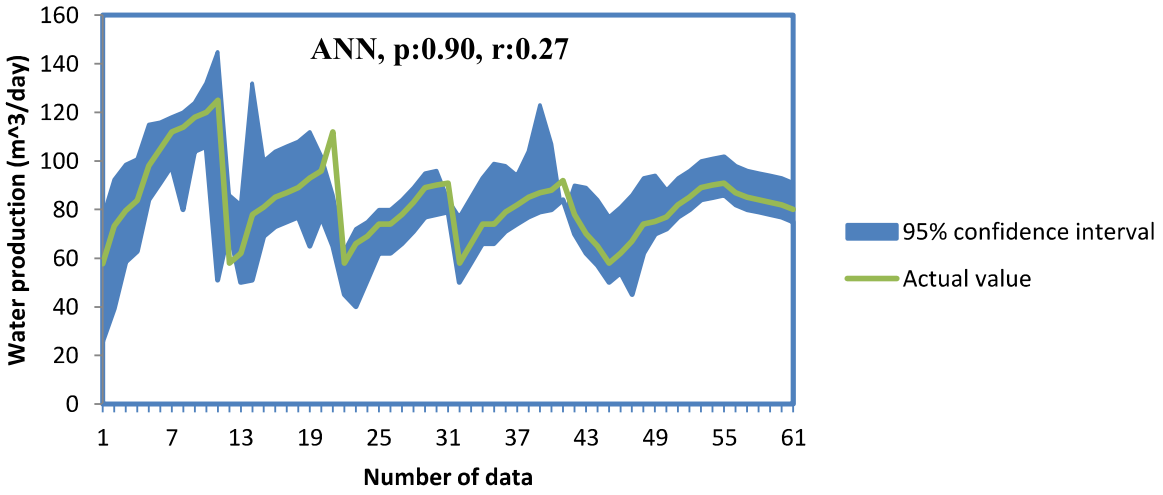

736

737 Figure 8. Uncertainty analysis of models based on the uncertainty of inputs to the models (the
738 first scenario)

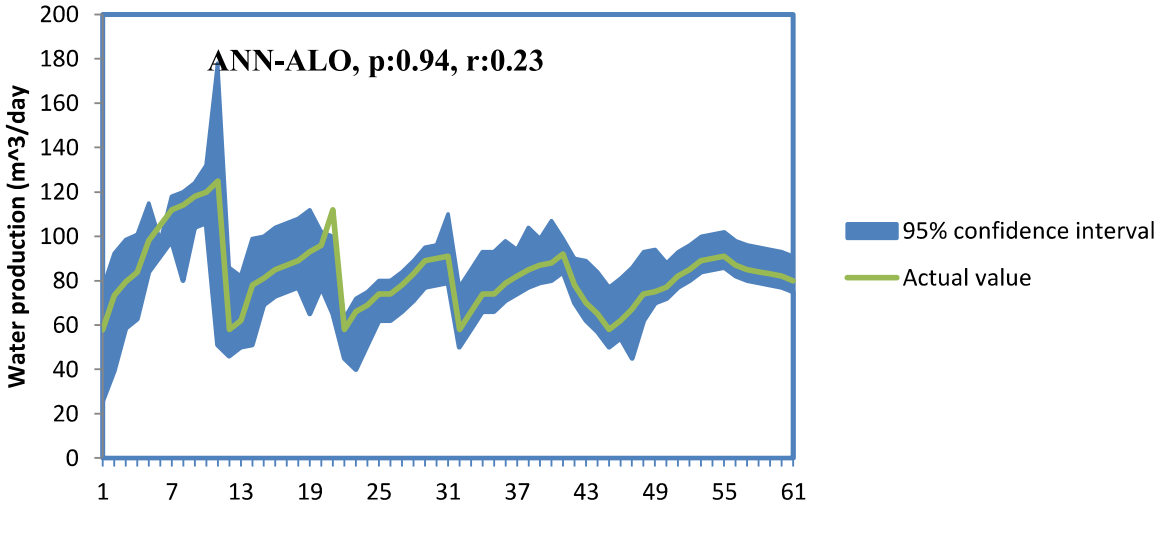
ANN-ALO, p:0.94, r:0.23
Water production (m^3/day
200
180
160
140
120
100
80
60
40
20
0
1
7
13
19
25
31
37
43
49
55
61
95% confidence interval
Actual value

739

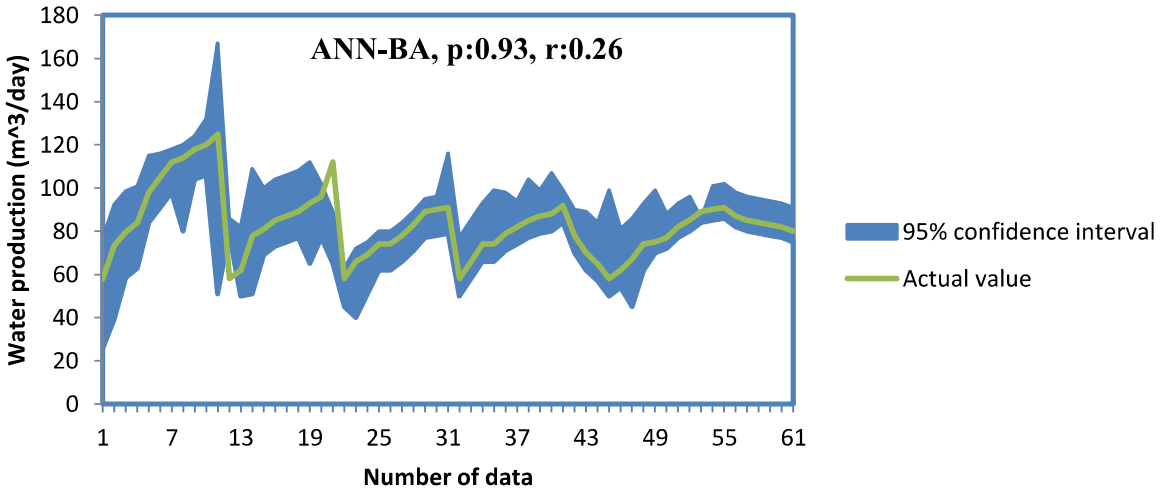
ANN-BA, p:0.93, r:0.26
Water production (m^3/day)
180
160
140
120
100
80
60
40
20
0
1
7
13
19
25
31
37
43
49
55
61
Number of data
95% confidence interval
Actual value

740

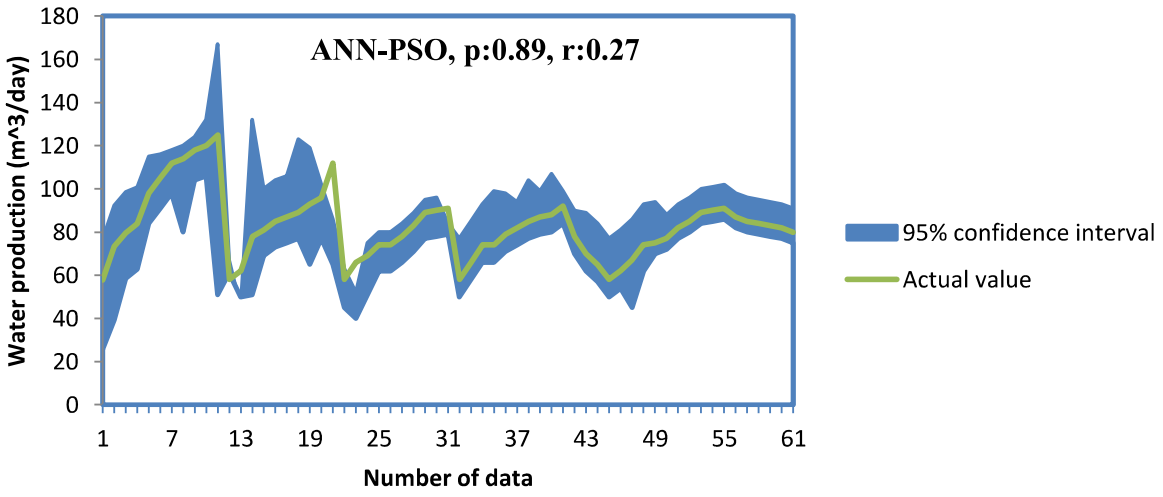
ANN-PSO, p:0.89, r:0.27
Water production (m^3/day)
180
160
140
120
100
80
60
40
20
0
1
7
13
19
25
31
37
43
49
55
61
Number of data
95% confidence interval
Actual value

741

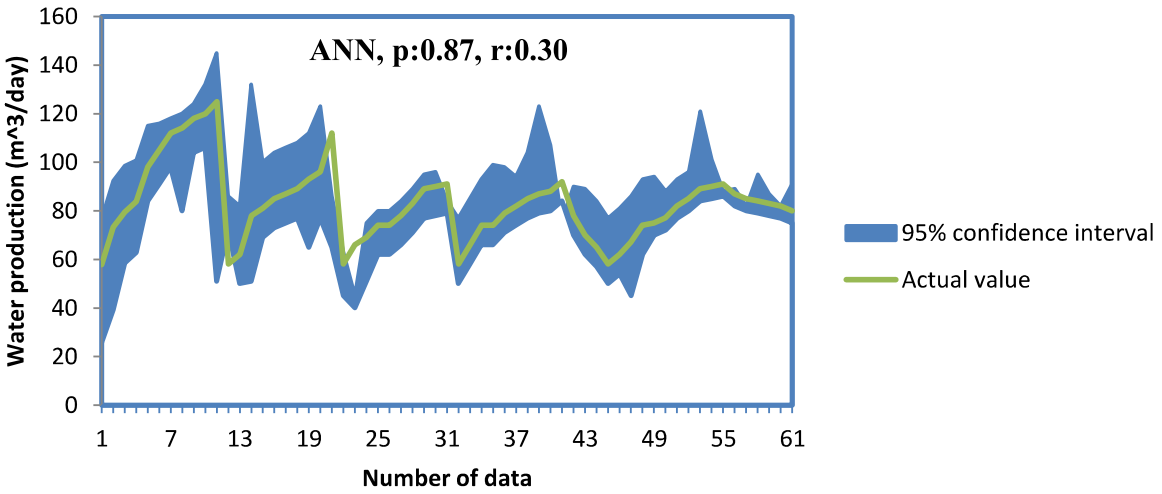

742

743 Figure 9. Uncertainty analysis of models based on the uncertainty of model parameters (the
744 second scenario)

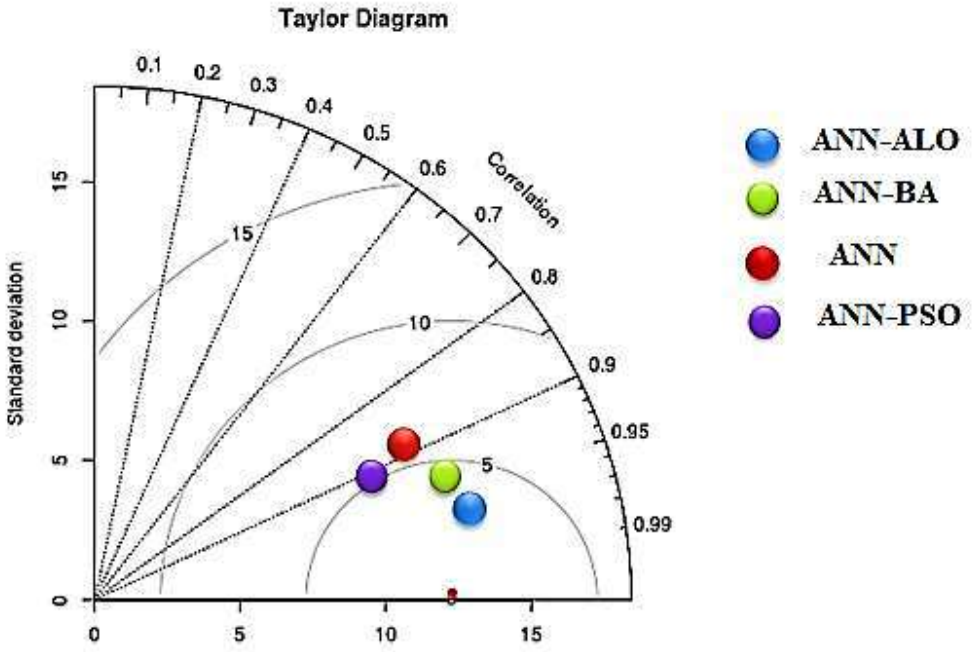

745

746 Figure 10. The Taylor digram for the models

747

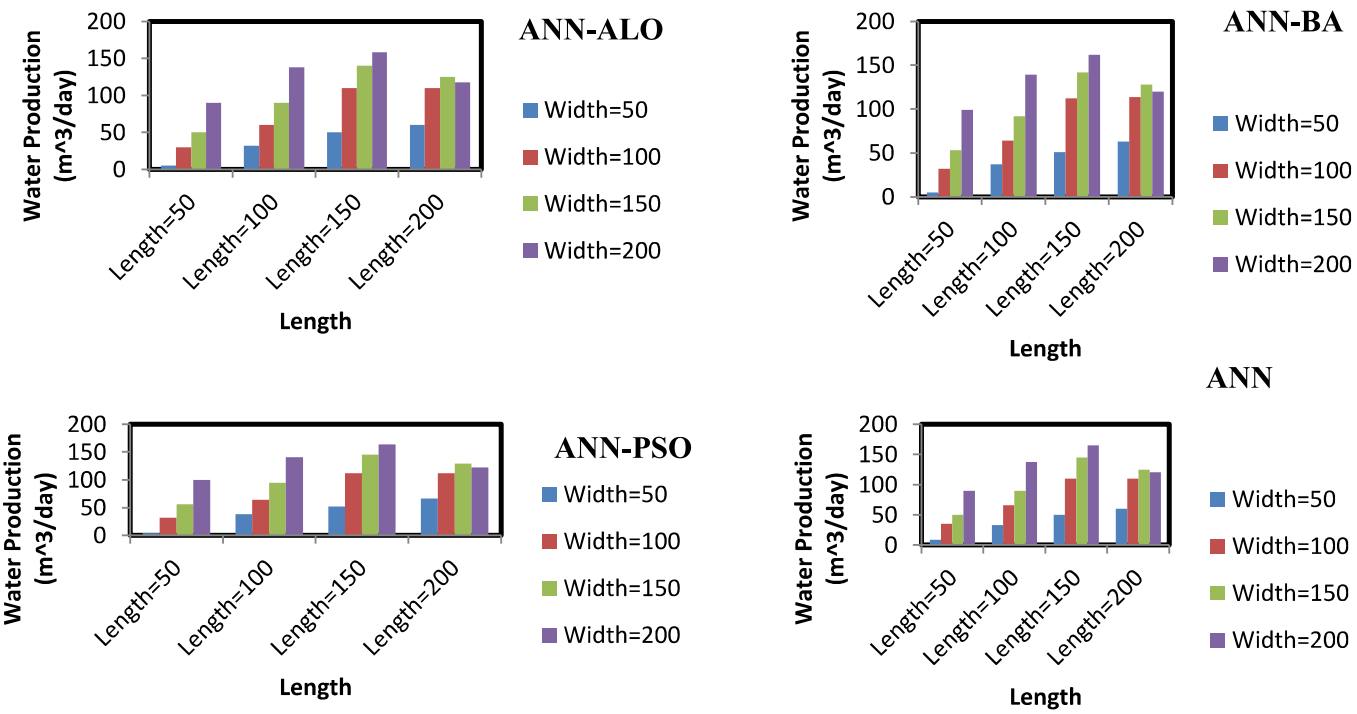

748

749 Figure 11. Investigation of the variation of width versus different lengths at the evaporator height
750 of 2m and transparency coefficient of 0.40

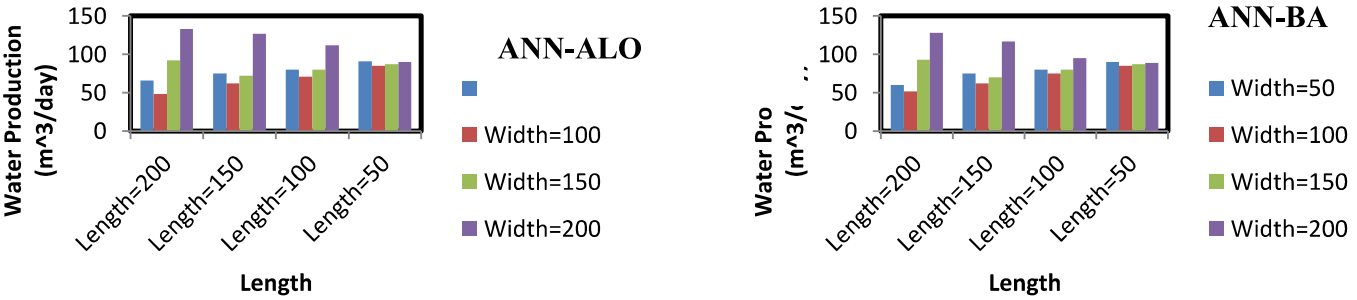

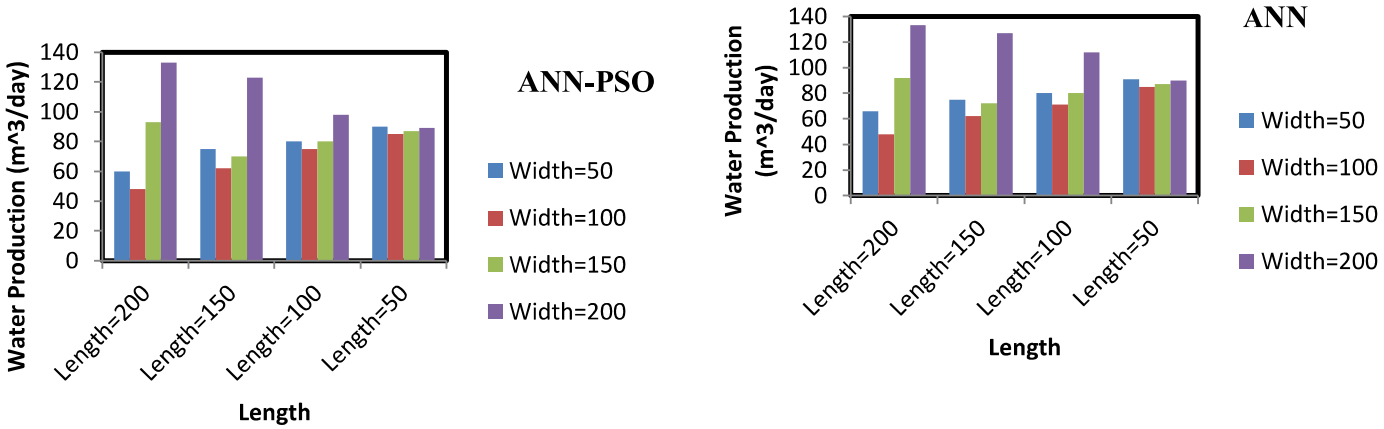

Figure 12. Investigation of the variation of width versus different lengths at the the evaporator height of 3m and transparency coefficient of 0.40

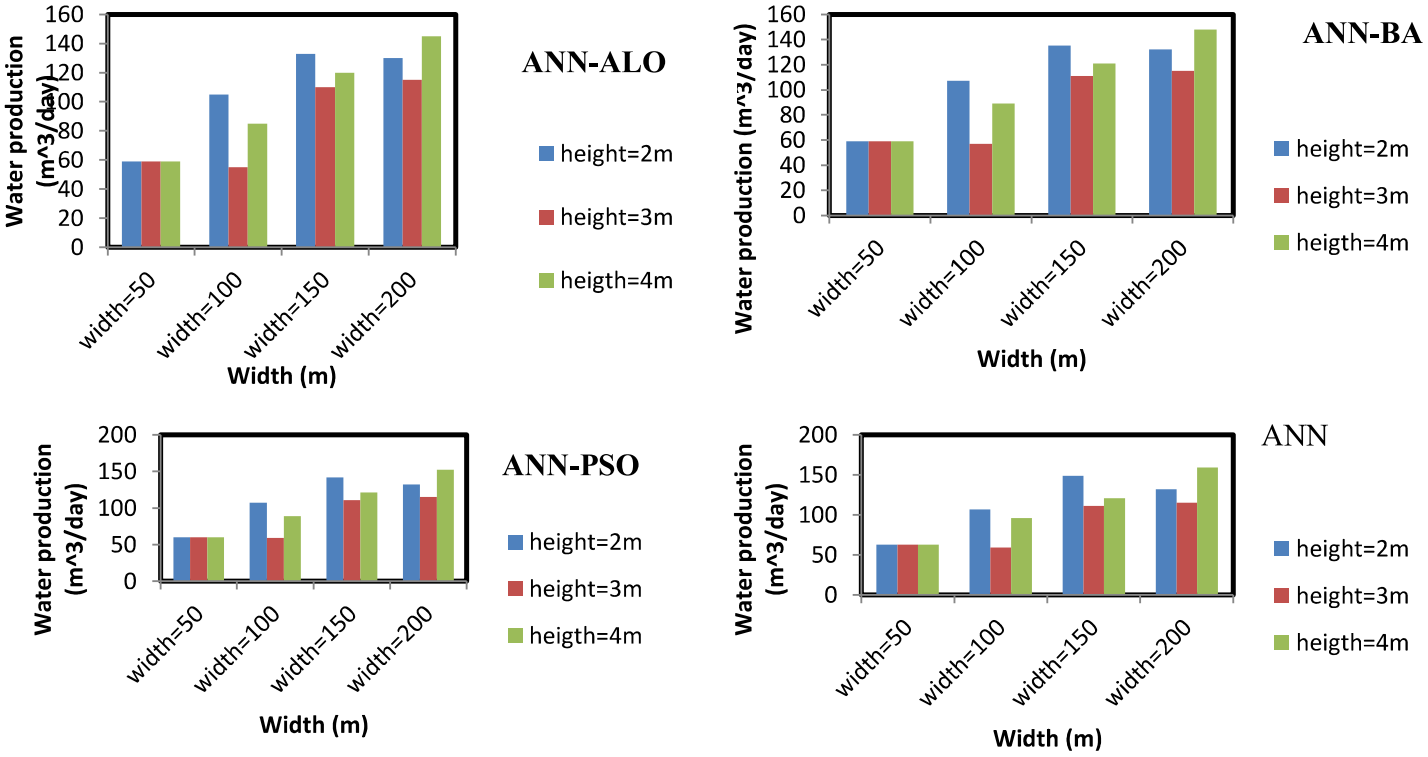

765

766

767 Figure 13. Investigation of the variation of height versus different widths on the water
768 production

769

770